




A novel synthesis of coral-like Co_3O_4 nanowires cluster for all-solid-state asymmetric supercapacitors

Wei Liu^{1,2} · Huailin Fan¹ · Jianyu Gu² · Donghong Wang² · Shijie Qu¹ 

Received: 25 January 2018 / Accepted: 16 March 2018 / Published online: 20 March 2018
© Springer Science+Business Media, LLC, part of Springer Nature 2018

Abstract

The coral-like Co_3O_4 nanowires (CNWs) cluster was synthesized by a novel strategy, in which polyurethane (PU) prepolymer was used as soft template during solvothermal process. The diameters of CNWs samples gradually decreased with the increasing of PU prepolymer. Electrochemical measurements showed that the CNWs possessed the largest specific capacitance of 502.6 F g^{-1} , which is 2.2 times higher than that of bulk Co_3O_4 . Moreover, an all-solid-state asymmetric supercapacitor based on CNWs as positive electrode and activated carbon as negative electrode delivered a high energy density of 18.3 Wh kg^{-1} and good cycling stability.

1 Introduction

Climate change and depletion of fossil fuels have stimulated intense concerns on energy storage systems, including batteries and capacitors [1]. In the recent years, supercapacitors have attracted huge attention due to their long cycle life, high power density and fast charge/discharge rates [2, 3]. However, using carbon materials as electrodes, conventional symmetric supercapacitors (SSCs) suffer from a limited energy density ($< 10 \text{ Wh kg}^{-1}$) [4, 5]. To solve this problem, an effective approach is to develop asymmetric supercapacitors (ASCs), in which either or both of two carbon electrodes are replaced by pseudocapacitive electrodes. ASCs can make full use of potential windows of two different electrodes to increase the operation voltage, resulting in higher energy density than SSCs [6–8]. Up to now, various redox-active materials have been employed as pseudocapacitive

electrode of ASCs, such as transition metal oxides [9–11]/hydroxides [12]/sulfides [13], conducting polymers [14] or metal–organic framework [15].

As a common transition metal oxide, Co_3O_4 has a wide application in catalysis [16], electrochemical capacitor [17, 18], batteries [19, 20] and wave absorption [21]; it is a promising candidate for positive electrode of ASCs due to its low cost, high redox activity and high theoretical specific capacitance [22, 23]. However, the electrochemical reaction between Co_3O_4 and electrolyte ions generally occurred in the surface layer of materials, which causes that bulk Co_3O_4 suffers from a limited specific capacitance due to low utilization ratio. Moreover, large volume change of Co_3O_4 during charging/discharging process causes a terrible cycling stability, which hinders its widespread application [24, 25]. To improve the utilization ratio of active materials, reducing the size of transition metal oxides to nanoscale is an accepted strategy [26]. Plenty of nanostructured Co_3O_4 with different morphologies are making its way into the material literature, including nanosheets [27], nanoplates [28], nanowires [29], nanocapsules [30], nanopolyhedrons [31] and nanoflowers [32]. Furthermore, one-dimensional materials can provide short transfer pathways for electron and remarkably accommodate the volume change caused by charging and discharging [33–35]. Therefore, it is anticipated that one-dimensional nanostructured Co_3O_4 would present higher specific capacitance and cycling stability in a high-performance supercapacitor. Hitherto, many efforts have been made to develop one-dimensional nanostructured Co_3O_4 . Hydrothermal method [36, 37] is the most common

Electronic supplementary material The online version of this article (<https://doi.org/10.1007/s10854-018-8944-0>) contains supplementary material, which is available to authorized users.

✉ Shijie Qu
qushijie2016@163.com

¹ State Key Laboratory of Coal Conversion, Institute of Coal Chemistry, Chinese Academy of Sciences, Taiyuan 030001, People's Republic of China

² Electromagnetic Protection Materials and Technology Key Laboratory of Shanxi Province, 33th Institute of China Electronics Technology Group Corporation, Taiyuan 030006, People's Republic of China

route to prepared Co_3O_4 nanowires. For example, Zhang et al. [36] deposited Co_3O_4 nanowires on Ni foam through a typical hydrothermal process assisted with NH_4F and urea. And various morphologies of Co_3O_4 nanowires could be controlled by adding different surfactants. In some reports [38, 39], Co_3O_4 nanowires were obtained by the conversion of precursor nanowires. Yao et al. [38] prepared Co_3O_4 nanowires through the decomposition of $\text{CoC}_2\text{O}_4 \cdot 2\text{H}_2\text{O}$ nanowires that were synthesized via a polyvinyl alcohol (PVA)-assisted co-precipitation process. The Co_3O_4 nanowires were also obtained by CVD [40] and hard template method [41].

Herein, we report a novel method to prepare coral-like Co_3O_4 nanowires (CNWs), in which polyurethane (PU) prepolymer was used as soft templates. To our best knowledge, there is no report on one-dimensional nanostructured metal oxides prepared by using PU prepolymer as template. The as-prepared CNWs exhibited high specific capacitance and excellent rate capability. All-solid-state ASCs were assembled by employing CNWs as positive electrode materials. The device showed a high energy density of 18.3 Wh kg^{-1} and long cycle life (83.6% retention after 5000 cycles).

2 Experimental

2.1 Materials

Polycaprolactone diol (PCL diol, $M_n = 2000$, Daicel, Japan) was dried and degassed at 80°C under vacuum for 3 h before use. Isophorone diisocyanate (IPDI, Aldrich) was dried over 4 \AA molecular sieves before use. Dimethylol butanoic acid (DMBA, Aldrich) was used as received. Urea and cobalt(II) nitrate ($\text{Co}(\text{NO}_3)_2 \cdot 6\text{H}_2\text{O}$) purchased from Shanghai Chemical Reagent Company were analytical grade. Activated carbon (AC) was prepared by KOH activation in our previous work [42].

2.2 Synthesis of polyurethane prepolymer

The preparation process of PU prepolymer was as follows: 0.012 mol PCL diol and 0.048 mol IPDI were introduced into a four-neck flask with mechanical stirrer, thermometer and reflux condenser. The reaction was carried out at 70°C under N_2 atmosphere for 2 h. After cooling to 50°C , 0.015 mol of DMBA was added into the flask. Then, reaction was maintained at 50°C for 4 h to prepare PU prepolymer.

2.3 Preparation of Co_3O_4 nanowires

The prepared PU prepolymer was added into acetone to obtain PU prepolymer solution. The concentration of solution was set

at 0, 0.5, 1 and 2 wt%. Subsequently, 30 g PU aqueous solution was mixed with 10 g of 30 wt% $\text{Co}(\text{NO}_3)_2 \cdot 6\text{H}_2\text{O}$ aqueous solution and 1 g of urea by magnetic stirring for 2 h. The mixture was then transferred into a Teflon-lined stainless steel autoclave (100 mL) and heated at 180°C for 24 h. The products were filtered, washed with ethanol and deionized water for several times and dried at 80°C for 12 h. Finally, the products were calcined at 400°C for 1 h in air to obtain Co_3O_4 nanowires. For convenience, the samples were denoted as CNW0, CNW0.5, CNW1 and CNW2, corresponding to the concentration of prepolymer solution.

2.4 Characterization

The microstructures and morphologies of the samples were observed by a field emission scanning electron microscopy (FE-SEM, JEOL JSM-7001F) and transmission electron microscope (TEM, JEM-2010). The crystallographic structure of cobalt oxide was investigated by X-ray diffraction (XRD, D8 Advance) equipped with $\text{Cu K}\alpha$ radiation. The elemental composition of the samples was detected by energy dispersive X-ray spectrometer (EDS). The X-ray photoelectron spectroscopy (XPS) spectra were performed on an AXIS ULTRAL DLD spectrometer with $\text{Al K}\alpha$ radiation. Nitrogen adsorption/desorption isotherms of the samples were collected using a Micromeritics ASAP 2020 adsorption apparatus.

2.5 Electrochemical measurements

The electrochemical performance was tested by an electrochemical workstation (CHI660E) in 6 M KOH solution. The working electrodes were fabricated by mixing active materials, carbon black and polytetrafluoroethylene (PTFE) in ethanol to form slurry with a weight ratio of 8:1:1. Then the slurry was applied to a piece of Ni foam, which was dried and pressed with another piece of Ni foam under 10 MPa subsequently. For three-electrode system, platinum foil and Hg/HgO electrode were selected as counter electrode and reference electrode, respectively. For two-electrode system, CNWs and AC were used as positive and negative electrode materials of all-solid-state ASCs. And KOH/polyvinyl alcohol (PVA) gel prepared by previous reports [43, 44] was selected as solid-state electrolyte.

The specific capacitance (F g^{-1}), energy density (Wh kg^{-1}) and power density (W kg^{-1}) of ASCs were calculated from follow equation [45].

$$C = \frac{I\Delta t}{m\Delta V} \quad (1)$$

$$E = \left(\frac{1}{2}\right) \left(\frac{1}{3.6}\right) C\Delta V^2 \quad (2)$$

$$P = \frac{I\Delta V}{2m} \quad (3)$$

where I represents charge/discharge current (A), Δt represents discharge time (s), m represents the total mass of active materials on two electrodes (g), and ΔV represents operation voltage (V).

3 Results and discussions

3.1 Structure characterization and formation mechanism of Co_3O_4 nanowires

The XRD patterns of CNWs are displayed in Fig. 1a. All samples exhibit eight obvious diffraction peaks at 2θ values of 19.0° , 31.3° , 36.9° , 38.6° , 44.9° , 55.7° , 59.3° and 65.2° , which matches well with the standard XRD pattern of the cubic spinel Co_3O_4 (JCPDS, no. 43-1003). No other obvious diffraction peaks are observed, indicating the high purity of samples. Moreover, diffraction peaks of Co_3O_4 become weaker slightly with the increasing of PU prepolymer concentration, which implies the decrease of crystallization. The EDS spectra were employed to investigate the elemental composition of the samples, as shown in Fig. S1. It can be seen that Co/O atomic ratios of all samples are close to 3:4, which reconfirms the existence of Co_3O_4 . There are not any carbon or nitrogen signals in the EDS spectra of all prepared CNWs samples, which implies that polyurethane prepolymer have been completely removed after thermal treatment. The XPS analysis is employed to further identify the valent state of cobalt (Fig. 1b). Two major peaks at 779.60 and 794.65 eV are displayed in Co 2p spectrum with spin-energy separation of 15.05 eV, which correspond to Co $2p_{1/2}$ and Co $2p_{3/2}$ of

Co_3O_4 , respectively. Moreover, two pairs of fitting peaks are ascribed to Co^{3+} (779.60 and 794.65 eV) and Co^{2+} (780.94 and 796.08 eV), respectively [46].

The SEM images of products prepared with various PU prepolymer solution concentrations are shown in Fig. 2. Without the assistant of PU prepolymer, CNW0 exhibits irregular bulk morphology (Fig. 2a). With the increasing of PU prepolymer concentration, the morphology of products is gradually converted into the interesting coral-like wires and the diameters of wires are gradually decreased from micrometers into nanometers (Fig. 2b, c, d). Nevertheless, the lengths of wires still retain around several tens of micrometers. As the concentration of prepolymer solution is 1 wt%, CNW1 exhibited Co_3O_4 wires with diameters of 300 nm and these nanowires are independent with each other (Fig. 3a). In the case of 2 wt% prepolymer solution, CNW2 shows smaller diameters of 100 nm and higher aspect ratio (Fig. 3b). However, the aggregation of nanowires for CNW2 is very obvious. As shown in Fig. 3c, TEM images of CNW2 reveals that Co_3O_4 nanowires have the diameters of about 100 nm, which is in agreement with the results of SEM. Moreover, it can be seen that nanowires are comprised of nanoparticles with the size of 20 nm. The lattice fringe spacing of 0.446 nm corresponds to the (111) crystal planes of cubic spinel Co_3O_4 (Fig. 3d), which is consistent with the XRD results.

According to SEM and TEM images, it is easy to conclude that PU prepolymer plays an important role in the formation of nanowires. The detail nucleation and growing mechanism of Co_3O_4 nanowires was illustrated in Fig. 4. Firstly, the PU prepolymer with abundant carboxyl groups was obtained from polymerization of PCL diol, IPDI and DMBA [47, 48]. Then, carboxyl groups on PU prepolymer chains could chelate Co^{2+} in the precursor solution to form Co^{2+} -PU complex. Furthermore, urea gradually

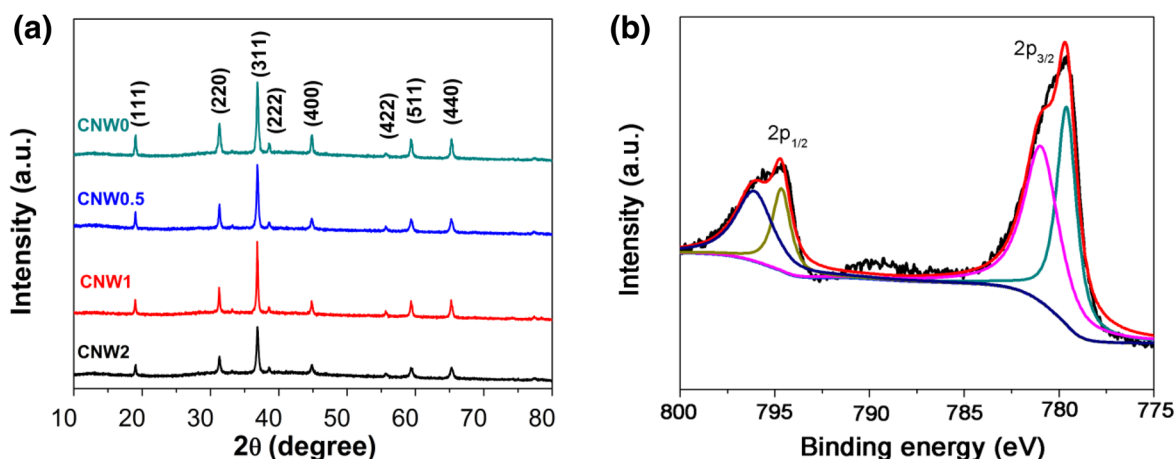


Fig. 1 a The XRD patterns of CNWs; b the XPS spectra of CNWs

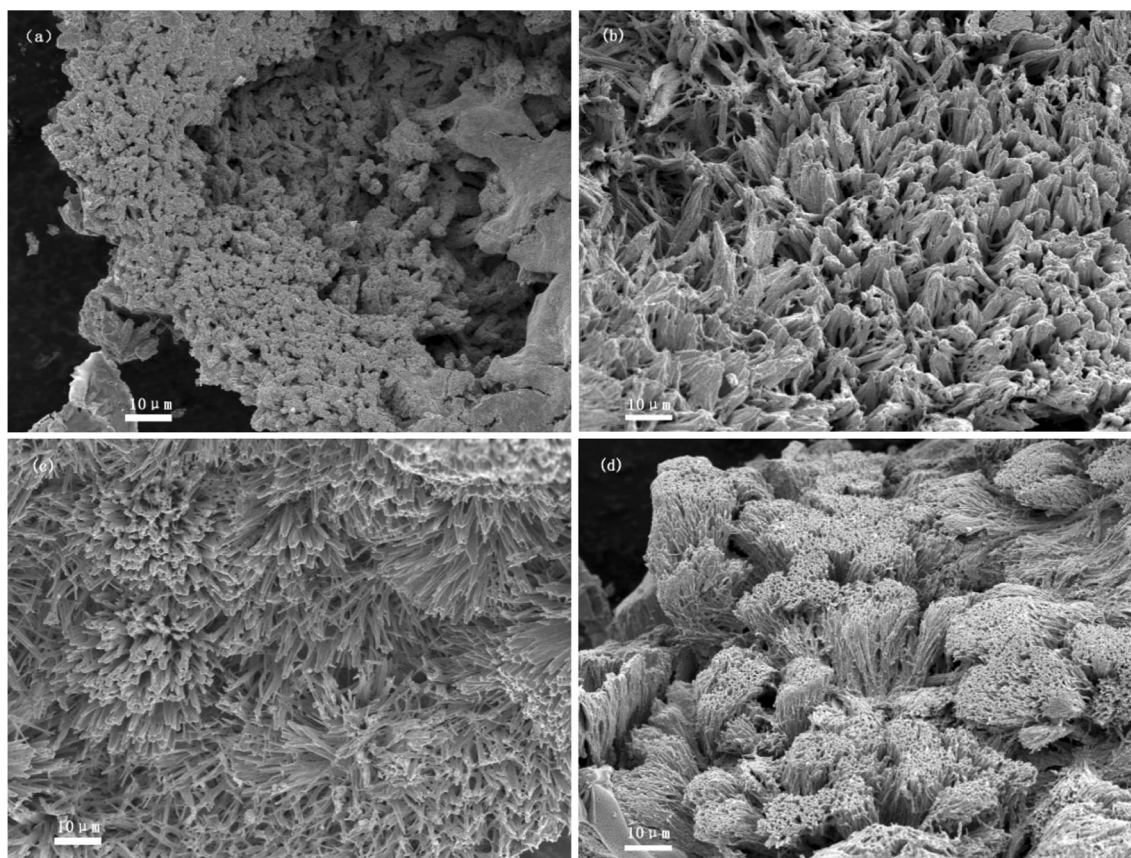
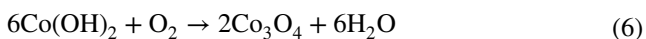
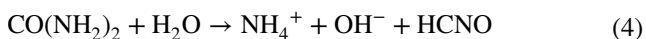


Fig. 2 The SEM images of **a** CNW0, **b** CNW0.5, **c** CNW1 and **d** CNW2

decomposed to release OH^- during the solvothermal process [Eq. (4)], which could react with Co^{2+} on PU prepolymer chains to obtain $\text{Co}(\text{OH})_2$ [Eq. (5)]. Finally, the Co_3O_4 nanowires were synthesized by thermal treatment in air [Eq. (6)].



The specific surface areas and pore-size distributions of the prepared products were obtained from N_2 adsorption/desorption isotherms (Fig. 5). Both products exhibit a type IV isotherm with a hysteresis loop at $0.7 < P/P_0 < 1.0$, indicating the existence of mesoporous structure that facilitates the diffusion of electrolyte ions. The pore-size distribution image calculated from BJH method further demonstrates that both products also have a narrow mesopore size distribution centered at 2.6 nm, which is originated from crevice of nanoparticles. However, Co_3O_4 nanowires present much larger nitrogen adsorption volume than bulk Co_3O_4 ,

suggesting the higher specific surface area and pore volume. The specific surface areas and pore volumes of CNWs are listed in Table 1. It can be observed that the specific surface area and pore volume are generally increased with the increasing of PU concentration. The specific surface area of CNW1 can reach $31.86 \text{ m}^2 \text{ g}^{-1}$, which is much larger than that of CNW0 ($9.49 \text{ m}^2 \text{ g}^{-1}$). With an exception, CNW2 possesses a lower specific surface area ($27.39 \text{ m}^2 \text{ g}^{-1}$) than CNW1, which may be caused by the aggregation of Co_3O_4 nanowires.

3.2 Electrochemical measurements

The electrochemical properties of the samples were first evaluated in a three-electrode system. To illustrate the advantage of nanowire-morphology, Fig. 6a compares the CV curves of CNWs with different microstructure at a scan rate of 10 mV s^{-1} . Clearly, the area of CV curves is dramatically enhanced when the morphology of Co_3O_4 is changed from bulks to wires, which could be attributed to the short

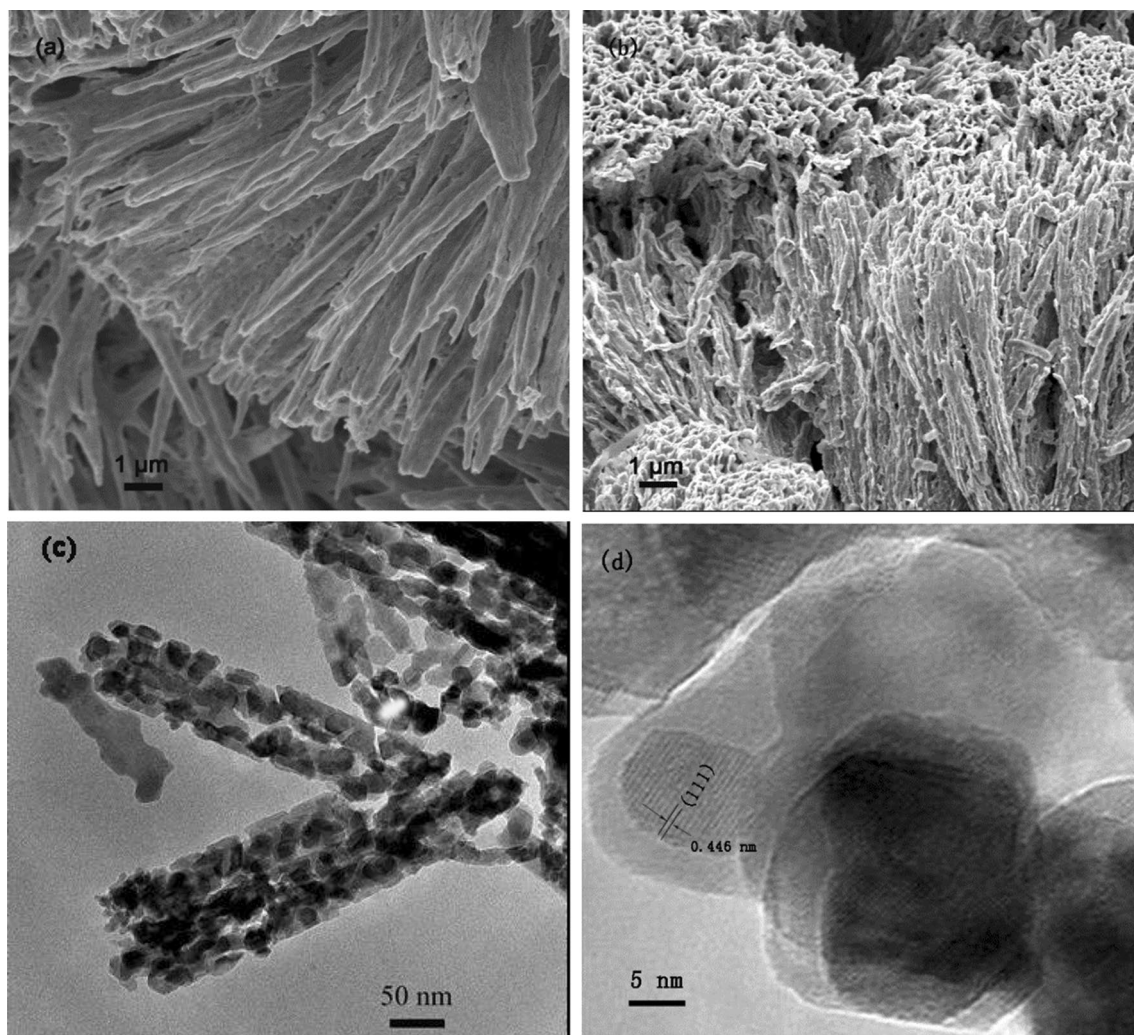


Fig. 3 The high resolution SEM images of **a** CNW1 and **b** CNW2; **c** TEM images of CNW2, **d** high resolution TEM images of CNW2

transfer pathways and the alleviation of the mechanical stress induced by the volume change during the charge/discharge processes for the 1D nanostructured materials. The CNW1 has the largest CV area, indicating a superior specific capacitance of CNW1, which could be attributed to higher specific surface area. Moreover, there are two pairs of redox peaks in the CV curves of Co_3O_4 , which can be ascribed to the conversions between various cobalt oxidation states as illustrated as follows [49]:

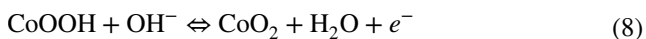


Figure 6b shows the CV curves of CNW1 at various scan rates. The shape of the CV curves has no obvious change with the increase of scan rate, which indicates that CNW1 displays high electrochemical reactivity. The oxidation and reduction peaks respectively shift to high potential and

low potential with the increase of scan rates, which can be attributed to irreversible reactions and electric polarization [50]. The galvanostatic charge/discharge curves of CNW1 at different current densities are presented in Fig. 6c. It can be seen that all charge/discharge curves are nonlinear lines and that there are two obvious voltage stages in the curves: 0–0.35 and 0.35–0.5 V, corresponding to the peaks in CV curves. The correlation between specific capacitance calculated according to Eq. (1) and current densities of CNWs is displayed in Fig. 6d. It can be observed that CNW1 possesses a high specific capacitance of 502.6 F g^{-1} at 0.5 A g^{-1} , which is about 2.2 times higher than that of bulk Co_3O_4 (225.9 F g^{-1}). Moreover, the specific capacitance of CNW1 can reach 466 F g^{-1} even at 10 A g^{-1} , which indicates the excellent rate capability.

Figure 6e shows the cycling stability of all CNWs samples at 5 A g^{-1} during 5000 charging/discharging cycles. It can be observed that CNW0, CNW0.5, CNW1, CNW2

Fig. 4 The detail nucleation and growing mechanism of Co_3O_4 nanowires

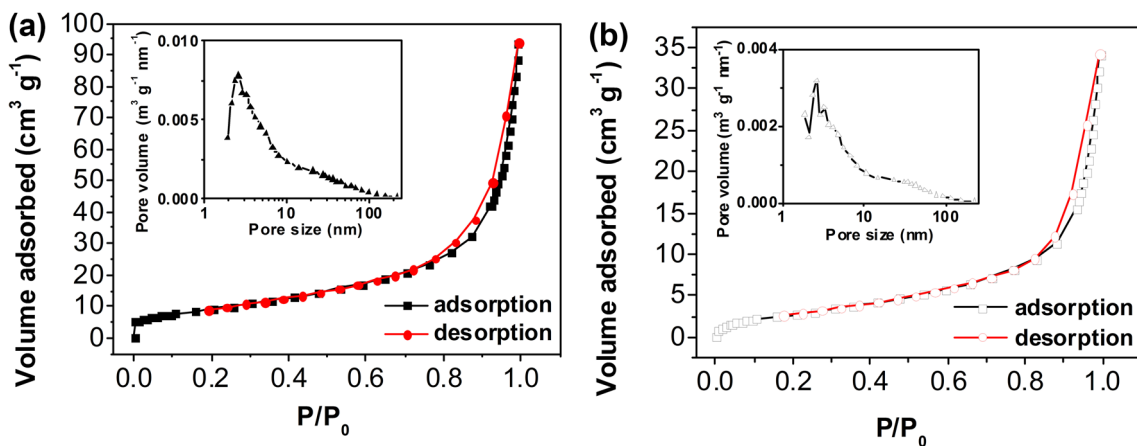
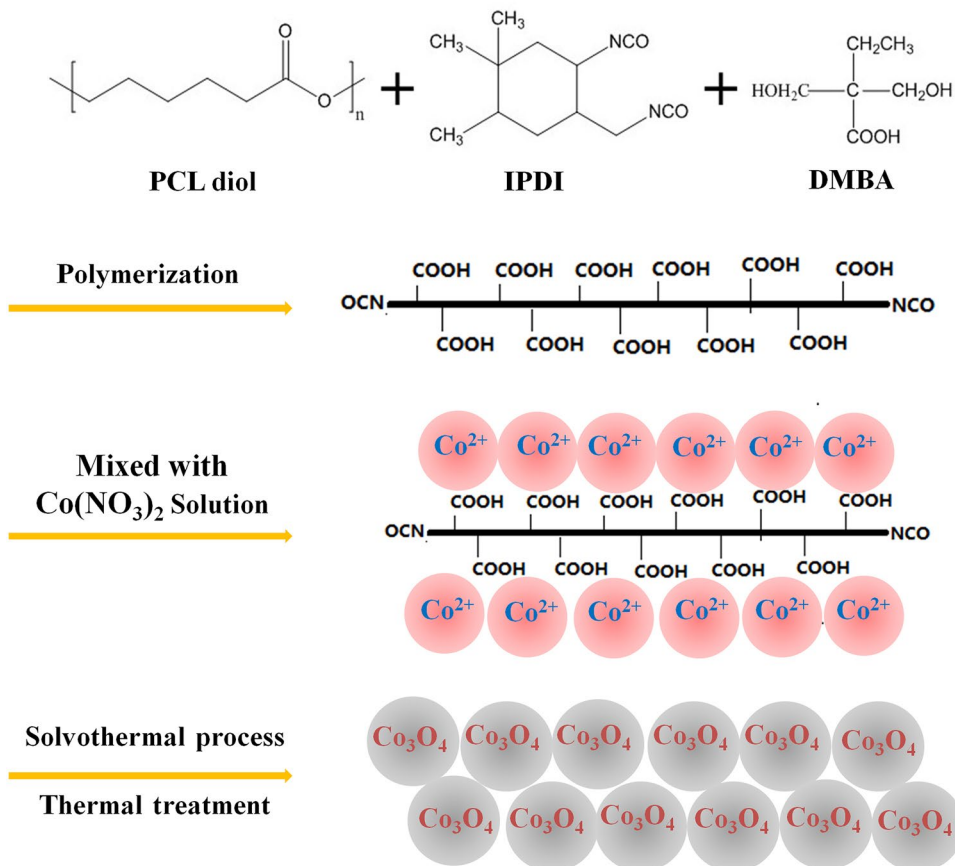


Fig. 5 The N_2 adsorption/desorption isotherms of **a** CNW1 and **b** CNW0. (The inset shows the pore size distribution of corresponding samples)

maintain 63.1, 75.8, 84.2 and 78.9% of their initial capacitance after 5000 cycles, respectively. This result demonstrates that Co_3O_4 nanowires possess higher cycling stability than that of bulk Co_3O_4 as we have mentioned above.

In order to investigate the practicability of as-prepared materials, asymmetric supercapacitors were assembled by using CNW1 as positive electrode and AC as negative electrode (denoted as CNWs//AC-ASC), respectively. And

Table 1 The specific surface areas and pore volumes of CNWs

Samples	S_{total} ($\text{m}^2 \text{g}^{-1}$)	S_{mesopore} ($\text{m}^2 \text{g}^{-1}$)	V_{total} ($\text{m}^3 \text{g}^{-1}$)	V_{mesopore} ($\text{m}^3 \text{g}^{-1}$)
CNW0	9.49	9.45	0.056	0.053
CNW0.5	19.73	19.67	0.075	0.072
CNW1	31.86	31.82	0.145	0.140
CNW2	27.39	27.33	0.136	0.129

S_{total} represents the total specific surface area of samples; S_{mesopore} represents the mesopore specific surface area of samples; V_{total} represents the total pore volume of samples; V_{mesopore} represents the mesopore pore volume of samples

KOH/PVA gel was adopted as solid electrolyte. As shown in Fig. 7a, the CNW1 electrode was measured within a stable potential window of 0–0.5 V whereas that of the AC electrode was measured from –1 to 0 V, which implies that asymmetric supercapacitors consisting of such two electrode can afford 1.5 V operation voltages in 6 M KOH aqueous electrolyte. To optimize the performance of the CNWs//AC-ASC, the charge between the positive and negative electrodes should be balanced. And the mass ratio of AC to CNWs is calculated to 1.06:1 according to follow equation [51]:

$$Q = mC\Delta V \quad (9)$$

where Q represents the charge on electrodes, m represents the mass of electrode materials, C represents the specific capacitance of electrode materials, and ΔV represents potential windows of electrode.

The CV curves of CNWs//AC-ASC with different operation voltages at 20 mV s^{-1} are displayed in Fig. 7b. When the operation voltage is ranged from 0.5 to 1.5 V, the type of CV curve is transformed from EDLC to pseudocapacitance, indicating that redox reaction occurred at high operation voltage. In any case, the results demonstrate that operation voltage of the assembled asymmetric supercapacitor can reach 1.5 V as we expected. The CV curves at various scan rates of CNWs//AC-ASC were performed between 0 and 1.5 V (Fig. 7c). With the increasing of the scan rates, the shape of the CV curves could still be well preserved, indicating fast charge/discharge rate. The GCD curves of CNWs//AC-ASC present a nearly symmetric shape (Fig. 7d), suggesting the good electrochemical reversibility and coulombic efficiency. In addition, the slight IR drop implies the low internal resistance of the device. Based on the total mass of active materials on two electrodes, the specific capacitance of CNWs//AC-ASC can reach 58.6 F g^{-1} at 1 A g^{-1} .

The energy density and power density of the device was further investigated according to Eqs. (2) and (3), and the Ragone plots are shown in Fig. 8a. The CNWs//AC-ASC exhibited a high energy density of 18.3 Wh kg^{-1} at a power density of 750 W kg^{-1} , which is much higher than that of conventional supercapacitors ($< 10 \text{ Wh kg}^{-1}$). The energy density of the device can still maintain 72% when power density is up to 7500 W kg^{-1} . These results are comparable to those of the recent reported all-solid-state supercapacitors [43, 52–57].

The cycling stability of the CNWs//AC-ASC was measured at 2 A g^{-1} . As shown in Fig. 8b, the specific capacitance of the device can still retain 83.6% of initial value after 5000 cycles, indicating the good cycling stability. Furthermore, three all-solid-state asymmetric supercapacitors in series can light a green LED under the original and bending states (inset of Fig. 8b), which reveals the structural integrity and practical application potential of the device.

4 Conclusions

The coral-like Co_3O_4 nanowires were prepared through solvothermal process and thermal treatment by using PU prepolymer as template. To our best knowledge, this novel route to prepare 1D nanostructured materials was reported for the first time. The formation mechanism of Co_3O_4 nanowires was also proposed. With the increasing of PU prepolymer, the diameters of as-prepared Co_3O_4 nanowires range from $1 \mu\text{m}$ to 100 nm . As electrode materials of supercapacitors, the CNWs exhibited a high specific capacitance of 502.6 F g^{-1} at 0.5 A g^{-1} in 6 M KOH solution, which was much larger than that of bulk Co_3O_4 . The excellent electrochemical performances could be attributed to short transfer pathways and the alleviation

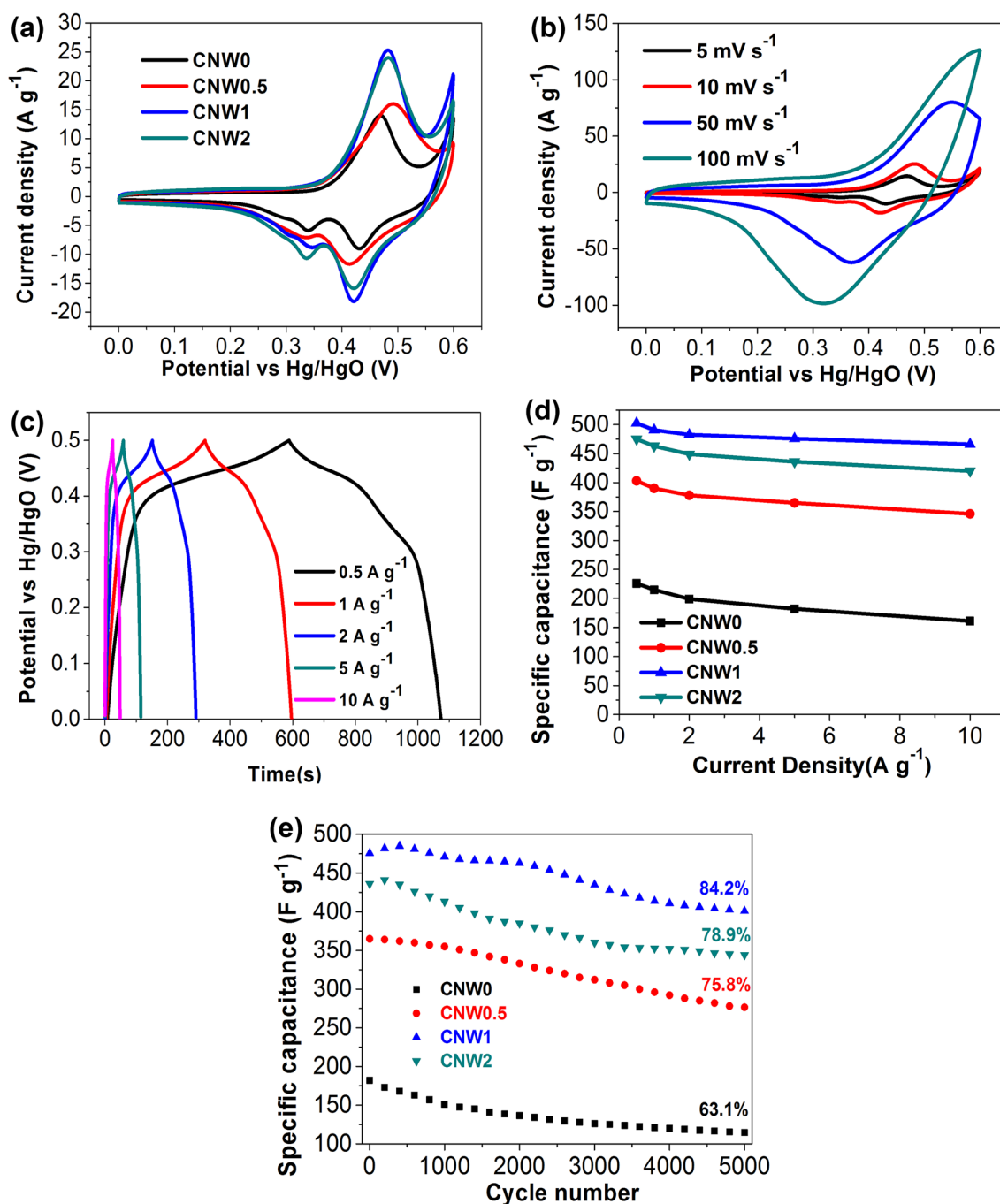


Fig. 6 **a** The CV curves of CNWs with different microstructure at a scan rate of 10 mV s^{-1} . **b** The CV curves of CNW1 at various scan rates. **c** The galvanostatic charge/discharge curves of CNW1 at different

current densities. **d** The correlation between specific capacitance and current densities of CNWs. **e** The cycling stability of CNWs at 5 A g^{-1} during 5000 charging/discharging cycles

of the mechanical stress produced by the volume change during the charge/discharge processes for the 1D nanostructured materials. The all-solid-state asymmetric supercapacitor assembled by using Co_3O_4 nanowires as positive

electrodes exhibited a high energy density of 18.3 Wh kg^{-1} and long cycle life along with 83.6% retention after 5000 cycles, which demonstrated its potential for application in energy storage.

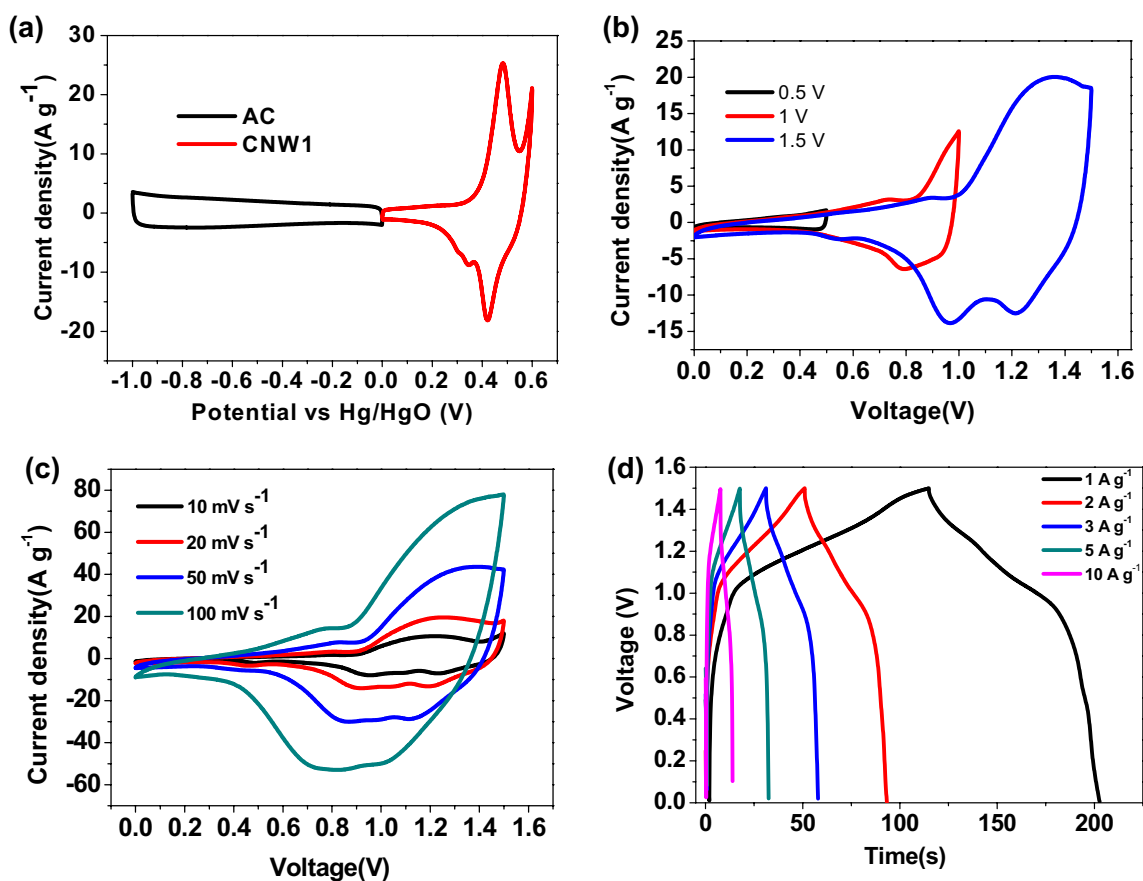


Fig. 7 **a** The CV curves of CNW1 and AC at different a scan rate of 10 mV s^{-1} . **b** The CV curves of CNWs//AC-ASC under different voltages. **c** The CV curves of CNWs//AC-ASC at different scan rates. **d** The GCD curves of CNWs//AC-ASC at different current densities

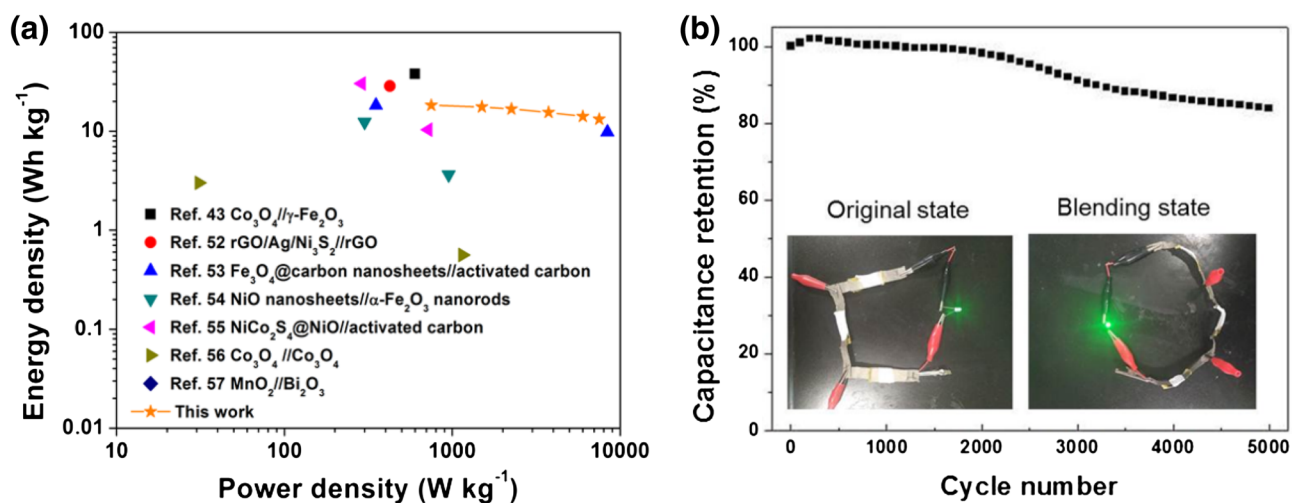


Fig. 8 **a** The Ragone plots of all-solid-state CNWs//AC-ASC compared with the recent reported all-solid-state supercapacitors. **b** The cycling stability of the CNWs//AC-ASC measured at 2 A g^{-1} after

5000 charging/discharging cycles. (The inset shows the optical images of a green lighted by three all-solid-state CNWs//AC-ASC in series)

Acknowledgements This study was supported by National Science Foundation of China (Nos. 21276266, U1510122 and U1710115).

References

1. Y. Zhang, S. Yu, G. Lou, Y. Shen, H. Chen, Z. Shen, S. Zhao, J. Zhang, S. Chai, Q. Zou, J. Mater. Sci. **52**, 11201 (2017)
2. F. Wang, X. Wu, X. Yuan, Z. Liu, Y. Zhang, L. Fu, Y. Zhu, Q. Zhou, Y. Wu, W. Huang, Chem. Soc. Rev. **46**, 6816 (2017)
3. A. González, E. Goikole, J.A. Barrena, R. Mysyk, Renew. Sustain. Energy Rev. **58**, 1189 (2016)
4. N. Goubard-Bretesche, O. Crosnier, F. Favier, T. Brousse, Electrochim. Acta **206**, 458 (2016)
5. D. Qu, L. Wang, D. Zheng, L. Xiao, B. Deng, D. Qu, J. Power Sources **269**, 129 (2014)
6. J. Yuan, S. Tang, Z. Zhu, X. Qin, R. Qu, Y. Deng, L. Wu, J. Li, G.M. Haarberg, J. Mater. Sci. Mater. Electron. **28**, 18022 (2017)
7. M. Qorbani, T. Chou, Y.H. Lee, S. Samireddi, N. Naseri, A. Ganguly, A. Esfandiari, C.H. Wang, L.C. Chen, K.H. Chen, A.Z. Moshfegh, J. Mater. Chem. A **5**, 12569 (2017)
8. S.K. Kiran, M. Padmini, H.T. Das, P. Elumalai, J. Solid State Electrochem. **21**, 927 (2017)
9. T. Liu, C. Jiang, W. You, J. Yu, J. Mater. Chem. A **5**, 8635 (2017)
10. R. Kumar, R.K. Singh, A.R. Vaz, R. Savu, S.A. Moshkalev, ACS Appl. Mater. Interfaces **9**, 8880 (2017)
11. R.J. Deokate, R.S. Kalubarme, C.J. Park, C.D. Lokhande, Electrochim. Acta **224**, 378 (2017)
12. L. Jiang, Y. Sui, J. Qi, Y. Chang, Y. He, Q. Meng, F. Wei, Z. Sun, Y. Jin, Part. Part. Syst. Character. **34**, 1600239 (2017)
13. Y. Zhu, X. Ji, Z. Wu, Y. Liu, Electrochim. Acta **186**, 562 (2015)
14. L. Zhang, D. Huang, N. Hu, C. Yang, M. Li, H. Wei, Z. Yang, Y. Su, Y. Zhang, J. Power Sources **342**, 1 (2017)
15. W. Xia, C. Qu, Z. Liang, B. Zhao, S. Dai, B. Qiu, Y. Jiao, Q. Zhang, X. Huang, W. Guo, D. Dang, R. Zou, D. Xia, Q. Xu, M. Liu, Nano Lett. **17**, 2788 (2017)
16. S. Xu, J. Tong, Y. Liu, W. Hu, G. Zhang, Q. Xia, J. Renew. Sustain. Energy **8**, 044703 (2016)
17. A.N. Naveen, P. Manimaran, S. Selladurai, J. Mater. Sci. Mater. Electron. **26**, 8988 (2015)
18. J. Xu, J. Cai, J. Wang, L. Zhang, Y. Fan, N. Zhang, H. Zhou, D. Chen, Y. Zhong, H. Fan, H. Shao, J. Zhang, C. Cao, Electrochim. Commun. **25**, 119 (2012)
19. M. Jing, M. Zhou, G. Li, Z. Chen, W. Xu, Z. Chen, Hou, ACS Appl. Mater. Interfaces **9**, 9662 (2017)
20. M. Yu, Z. Wang, C. Hou, Z. Wang, C. Liang, C. Zhao, Y. Tong, X. Lu, S. Yang, Adv. Mater. **29**, 1602868 (2017)
21. G. Wang, Y. Wu, Y. Wei, X. Zhang, Y. Li, L. Li, B. Wen, P. Yin, L. Guo, M. Cao, ChemPlusChem **79**, 375 (2014)
22. V.H. Nguyen, J.J. Shim, Mater. Lett. **157**, 290 (2015)
23. W. Liu, H. Fan, W. Shen, S. Qu, ChemistrySelect **1**, 6469 (2016)
24. Y. You, M. Zheng, L. Ma, X. Yuan, B. Zhang, Q. Li, F. Wang, J. Song, D. Jiang, P. Liu, L. Ma, W. Shen, Nanotechnology **28**, 105604 (2017)
25. C. Feng, J. Zhang, Y. He, C. Zhong, W. Hu, L. Liu, Y. Deng, ACS Nano **9**, 1730 (2015)
26. M. Aghazadeh, I. Karimzadeh, M.R. Ganjali, A. Behzad, J. Mater. Sci. Mater. Electron. **28**, 18121 (2017)
27. R. Wang, J.Q. Qi, Y.W. Sui, Y. Chang, Y.Z. He, F.X. Wei, Q.K. Meng, Z. Sun, Y.L. Zhao, Mater. Lett. **184**, 181 (2016)
28. P. Razmjoo, B. Sabour, S. Dalvand, M. Aghazadeh, M.R. Ganjali, J. Electrochem. Soc. **161**, D293 (2014)
29. M. Fan, B. Ren, L. Yu, D. Song, Q. Liu, J. Liu, J. Wang, X. Jing, L. Liu, Electrochim. Acta **166**, 168 (2015)
30. M. Aghazadeh, M. Hosseinfard, B. Sabour, S. Dalvand, Appl. Surf. Sci. **287**, 187 (2013)
31. X. Liu, F.X. Wei, Y.W. Sui, J.Q. Qi, Y.Z. He, Q.K. Meng, J. Alloys Compd. **735**, 1339 (2018)
32. Q. Balouch, Z.H. Ibupoto, G.Q. Khaskheli, R.A. Soomro, M.K. Sirajuddin, V.K. Samoon, Deewani, J. Electron. Mater. **44**, 3724 (2015)
33. S. Sun, X. Zhao, M. Yang, L. Ma, X. Shen, Nanomaterials **5**, 2335 (2015)
34. A.K. Nayak, A.K. Das, D. Pradhan, ACS Sustain. Chem. Eng. **5**, 10128 (2017)
35. X. Liu, Z. Wu, Y. Yin, Chem. Eng. J. **323**, 330 (2017)
36. X. Zhang, Y. Zhao, C. Xu, Nanoscale **6**, 3638 (2014)
37. L. Gao, S. Xu, C. Xue, Z. Hai, D. Sun, Y. Lu, J. Nanopart. Res. **18**, 112 (2016)
38. X. Yao, X. Xin, Y. Zhang, J. Wang, Z. Liu, X. Xu, J. Alloys Compd. **521**, 95 (2012)
39. J.W. Kim, J.K. Lee, D. Pihusut, Y. Yi, H.J. Lee, J. Lee, J. Phys. Chem. C **117**, 23712 (2013)
40. M. Bueyekyazi, C. Hegemann, T. Lehnen, W. Tyrra, S. Mathur, Inorg. Chem. **53**, 10928 (2014)
41. G.B. Ji, Z.H. Gong, W.X. Zhu, M.B. Zheng, S.T. Liao, K. Shen, J.S. Liu, J.M. Cao, J. Alloys Compd. **476**, 579 (2009)
42. H. Fan, W. Liu, W. Shen, Chem. Eng. J. **326**, 518 (2017)
43. R. Wang, Y.W. Sui, S.F. Huang, Y.G. Pu, P. Cao, Chem. Eng. J. **331**, 527 (2018)
44. X. Xu, J. Gao, Q. Tian, X. Zhai, Y. Liu, Appl. Surf. Sci. **411**, 170 (2017)
45. D. Yan, H. Zhang, L. Chen, G. Zhu, S. Li, H. Xu, A. Yu, ACS Appl. Mater. Interfaces **6**, 15632 (2014)
46. Q. Ke, C. Tang, Z. Yang, M. Zheng, L. Mao, H. Liu, J. Wang, Electrochim. Acta **163**, 9 (2015)
47. S.H. Yoon, J.H. Park, E.Y. Kim, B.K. Kim, Colloid Polym. Sci. **289**, 1809 (2011)
48. Y.J. Kim, B.K. Kim, Colloid Polym. Sci. **292**, 51 (2014)
49. M. Aghazadeh, R. Ahmadi, D. Gharailou, M.R. Ganjali, P. Norouzi, J. Mater. Sci. Mater. Electron. **27**, 8623 (2016)
50. L. Fan, L. Tang, H. Gong, Z. Yao, R. Guo, J. Mater. Chem. **22**, 16376 (2012)
51. Q. Li, Y. Li, H. Peng, X. Cui, M. Zhou, K. Feng, P. Xiao, J. Mater. Sci. **51**, 9946 (2016)
52. J.Q. Qi, Y. Chang, Y.W. Sui, Y.Z. He, Q.K. Meng, F.X. Wei, Y.J. Ren, Y.X. Jin, Adv. Mater. Interfaces **5**, 1700985 (2017)
53. H. Fan, R. Niu, J. Duan, W. Liu, W. Shen, ACS Appl. Mater. Interfaces **8**, 19475 (2016)
54. S. Zhang, B. Yin, Z. Wang, F. Peter, Chem. Eng. J. **306**, 193 (2016)
55. Y. Huang, T. Shi, S. Jiang, S. Cheng, X. Tao, Y. Zhong, G. Liao, Z. Tang, Sci. Rep. **6**, 38620 (2016)
56. X.Y. Liu, Y.Q. Gao, G.W. Yang, Nanoscale **8**, 4227 (2016)
57. H. Xu, X. Hu, H. Yang, Y. Sun, C. Hu, Y. Huang, Adv. Energy Mater. **5**, 1401882 (2015)